THE JOURNAL OF PHYSICAL CHEMISTRY C

pubs.acs.org/JPCC Article

Charge Transport Mechanism in Chevron-Graphene Nanoribbons

Marcelo Lopes Pereira Júnior, Wiliam Ferreira da Cunha, Rafael Timóteo de Sousa Junior, William Ferreira Giozza, Geraldo Magela e Silva, and Luiz Antônio Ribeiro Junior*

Cite This: J. Phys. Chem. C 2020, 124, 22392−22398 Read Online

ACCESS | Metrics & More | Article Recommendations | Supporting Information

ABSTRACT: From the moment atomic precision control of the growth process of graphene was achieved, more elaborated carbon allotropes were proposed opening new channels for flat optoelectronics at the nanoscale. A special type of this material presenting a V-shape (or "kinked" pattern) was recently synthesized and named chevron-graphene nanoribbons (C-GNRs). To realize the reach of C-GNRs in developing new applications, the formation and transport of charge carriers in their lattices should be primarily understood. Here, we investigate the static and dynamical properties of quasiparticles in C-GNRs. We study the effects of electron−phonon coupling and doping on the system. We also determine the kind of charge carriers present in C-GNR. Two distinct physical pictures for the charge transport were obtained: a delocalized regime of conduction and a regime mediated by charge carriers. These transport regimes are highly dependent on the doping concentration. Importantly, similarities in charge carrier terminal velocities were observed among C-GNRs and standard armchair graphene nanoribbons, which originate from their comparable charge localization profiles that yield quasiparticles with equivalent effective masses.

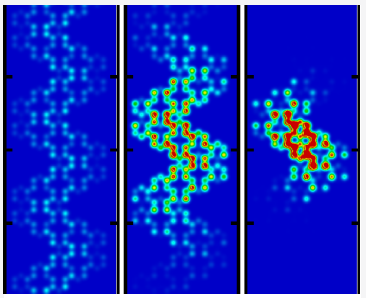

Atomic charge density for different coupling values between electrons and lattice phonons.

INTRODUCTION

Molecular electronics is currently a field attracting the attention of the scientific community for the potential it presents of giving rise to low-cost energy-efficient devices. Organic systems, in particular, are the most promising source of materials to spawn a molecular electronic revolution. This feature is due to the cost-efficient nature of the material as well as the similarities between carbon and silicon on which the current electronic industry is based.

Among the several possible organic systems in the electronic industry, the synthesis of graphene quickly defined it as the most promising one.[1,2] Being a true two-dimensional (2D) system, it provides a large surface-to-volume ratio for several applications. Also, the possibility of roll-to-toll processing[3] resulted in the proposal of a large range of ideas.[4] As a major drawback, though, the pristine two-dimensional graphene sheet lacks the band gap typical of the conventional semiconductors.[5,6] Several different procedures have been employed to circumvent this difficulty. The main one is to resort to graphene-based systems with different topological structures. Different allotropes have been extensively studied, among which are carbon nanotubes[7] and nanoribbons.[8] The change in physical structure results in changes in the band structure of the materials, which manifests as rising of interesting, frequently tunable, electronic and transport properties.

The control of the precision of width, edge structure, stacking, and growth process leads to more elaborated classes of graphene-based systems, opening a whole new range of possibilities. Carbon nanoscrolls,[9] popgraphene,[10] phagraphene,[11] pentagraphene,[12] and chevron-graphene[13−18] nanoribbons (C-GNRs) are among the new candidates. In recent years, this latter species has been the subject of major interest. It consists of a special type of graphene nanoribbon that presents a V-shape, or "kinked" pattern. It can be reasoned to be formed from the periodic juxtaposition of two angularly shifted armchair graphene nanoribbons, displaced as shown in Figure 1.

Recent experimental evidence suggests C-GNRs as promising materials for applications in organic electronics and photovoltaics.[19] Several other works have dealt with the synthesis of C-GNR.[19−26] Some studies have shown that C-GNRs share interesting properties that arise in different carbon allotropes while presenting other unique features.[27,28] Finally, possible applications of C-GNRs in heterojunctions have also already been reported.[29] However, so far, the literature lacks the theoretical description of its electronic and transport properties. This fact results in controversies in elementary, yet fundamental, characteristics of the system. Therefore, an extensive study describing how electronic transport takes place in C-GNRs is paramount to the further development of molecular electronics. Of particular importance is to highlight

Received: July 20, 2020
Revised: September 22, 2020
Published: September 24, 2020

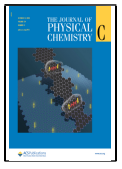

https://dx.doi.org/10.1021/acs.jpcc.0c06625
J. Phys. Chem. C 2020, 124, 22392−22398

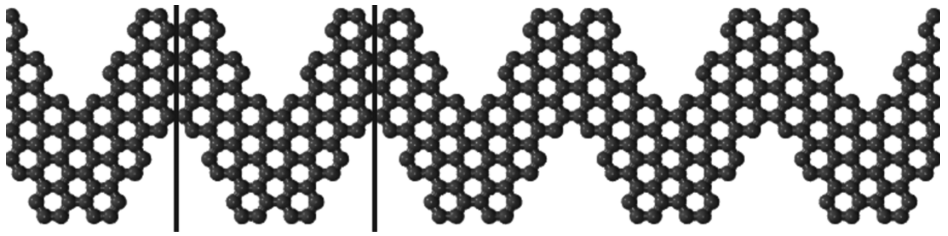

Figure 1. Structural representation of a chevron-graphene nanoribbon. A unit cell is highlighted.

the differences between the transport phenomena in C-GNRs and those observed in regular armchair graphene nanoribbons.

Herein, we make use of a 2D tight-binding Hamiltonian, which includes lattice relaxation effects to discuss the electronic and transport properties in C-GNRs. We start by conducting a set of simulations to determine the electron−phonon coupling strength. Next, we analyze how different electron−phonon coupling constants contribute to the appearance of quasiparticles. We discuss both the static and dynamical properties of different quasiparticles under the effect of an external electric field. This description is expected to give important insights for improving the performance of electronic devices based on C-GNRs, such as heterojunctions.

METHODS

The model implemented to investigate the electronic and transport properties of C-GNRs is based on a 2D SSH-type Hamiltonian[30,31] endowed with lattice relaxation. In it, we describe the electronic degrees of freedom of the system quantum mechanically in a second quantization formalism, whereas the lattice is treated classically by employing a set of Euler−Lagrange equations. It should be noted, however, that these two realms are coupled so that the problem ought to be solved self-consistently.

The coupling between the electronic and lattice degrees of freedom is implemented in the electronic transfer integrals, which are expressed in such a way that the hopping of electrons between sites depends on the lattice disposition. In the case of covalent C−C bonds, the lattice displacement is a small fraction of the equilibrium size (usually not much higher than 2%). This justifies the use of a first-order expansion for the electronic transfer integral of π-electrons dependence on the displacement.[32]

Figure 2a shows the unit cell of a C-GNR lattice. The zoomed panel (Figure 2a) clarifies the labeling of the sites. Let $\eta_{i,j}$ be the variations in the bond lengths between two neighboring sites i and j. From the previous considerations, the expanded transfer integral to be plugged into our model Hamiltonian takes the form

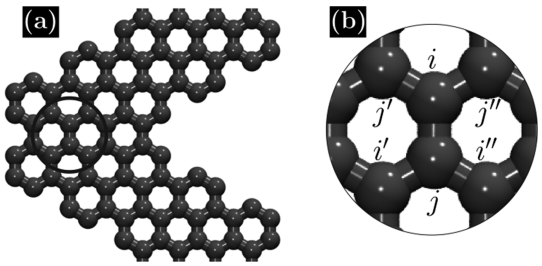

Figure 2. (a) Unit cell of a chevron-graphene nanoribbon and (b) highlight presenting site labeling.

$$t_{i,j} = t_0 - \alpha\eta_{i,j} \tag{1}$$

t_0 is the hopping integral that the evenly spaced system would have in a pure tight-binding model. α is the aforementioned coupling constant, responsible for the coupling between electrons and phonons.

In this approach, the model Hamiltonian of the system is given by

$$H = -\sum_{\langle i,j\rangle,s} (t_{i,j}C_{i,s}^{\dagger}C_{j,s} + t_{i,j}^{*}C_{j,s}^{\dagger}C_{i,s}) + \frac{1}{2}K\sum_{\langle i,j\rangle}\eta_{i,j}^{2} + \frac{1}{2M}\sum_{i}p_{i}^{2} \tag{2}$$

Here, $\langle i, j\rangle$ represents the sum carried out on neighboring sites.[30,31] $C_{i,s}$ stands for the π-electron annihilation operator on site i with spin s and $C_{i,s}^{\dagger}$ represents its hermitian conjugate, i.e., the corresponding creation operator. The remaining terms express the lattice degrees of freedom of the system. The second term is a harmonic approximation to model the effective potential associated with σ-bonds between carbon atoms, K being the elastic constant. The last term expresses the kinetic energy of the sites in terms of their momenta $_{pi}$ and mass M of the carbon cores. One should note that, as the transfer integral is position-dependent, the movement of the sites indeed impacts the behavior of the electrons. This reason dictates that the lattice and the electron parts of the problem must be solved simultaneously in a self-consistent fashion, as previously argued.

Following previous theoretical and experimental works,[33−43] the values of the model parameters were set to be 2.7 eV for t_0 and 21 eV/Å^2 for K. As for the α, the nature of the present contribution dictates that we should perform a specific search of the suitable values by considering the range from 0.1 to 6.0 eV/Å. In this sense, the most suitable electron−phonon coupling value was obtained using a tuning procedure[44] that contrasted the highest occupied molecular orbital−lowest energy unoccupied molecular orbital (HOMO−LUMO) gaps calculated here for both C-GNR and E-GNR with the experimental band gap values reported in ref 14. The ground state solutions and the time evolution of the system are obtained by employing the procedures described in the refs 45 and 46.

RESULTS AND DISCUSSION

Here, we describe a symmetric C-GNR (Figure 1). The total length of the unit cell is set to be 144 Å, and periodic boundary conditions were applied in this direction. For the sake of clarity, we depict the C-GNRs as simple rectangular stripes, although the actual simulations were performed with the proper topology of the system shown above.

https://dx.doi.org/10.1021/acs.jpcc.0c06625
J. Phys. Chem. C 2020, 124, 22392−22398

We begin our discussions by investigating the crucial aspect of the electron−phonon coupling constant value to be employed in our simulations. Our procedure is to tune the value of this constant having the energy gap of the system as a parameter. Indeed, the energy gap is the experimental property most convenient in determining the electron−phonon coupling value. The energy gap is related to both the geometric disposition, which is a clear lattice property, and the electronic distribution. The energy gap also has an important influence on the electronic properties of the system, as we shall see below.

Although the energy gaps of C-GNRs, and laterally extended chevron-graphene nanoribbons (E-GNRs), are still a subject of some debate in the literature, the accepted values vary from 1.6 to 3.2 eV.[13,14] Here, we choose the results for the most usual substrate as the reference values to set up the electron−phonon coupling strength.[14] For C-GNR and E-GNR, the reference values are 2.76 ± 0.3 and 2.66 ± 0.5 eV,[14] respectively. In our calculations, the adopted set of model parameters yielded band gaps of 2.28 and 2.04 eV for C-GNR and E-GNR, respectively. For the sake of convenience, the Supporting Information presents the results obtained for E-GNR systems once they are very similar to those of the related C-GNR ones.

Slight discrepancies in the energy gap can be attributed to impurities, topology of the system, strain, substrate, and other external factors. Therefore, even though the reference value of 2.76 ± 0.3 eV[14] is reliable, other values, as long as sufficiently close to this one, should also be considered, as they might be representatives of the system under slightly different conditions.

Now that a suitable range for the electron−phonon constant (α) is defined, we consider charge carriers in our simulations. The first step in this direction is to simulate the system with a net positive charge and to describe how the charge is distributed throughout the two-dimensional lattice. This is accomplished by extracting one electron from the C-GNR lattice and to compute the inverse participation ratio (IPR), which is a measure of the degree of charge localization, commonly used to define the nature of quasiparticles[47]

$$\mathrm{IPR} = \frac{\sum_{i,j} |\rho_{i,j}|^2}{\left(\sum_{i,j} |\rho_{i,j}|\right)^2} \tag{3}$$

IPR is a dimensionless quantity that varies from 0.0 in the case of a completely delocalized charge to 1.0 associated with complete localization. Figure 3a presents the result of the system's IPR for different α constants considered in this work, and Figure 3b−d illustrates the atomic charge density profiles for C-GNR lattices considering representative electron−phonon coupling cases. In Figure 3a, we show the behavior of the IPR as a function of α. As is the case in many extended organic systems, our simulations presented relatively small values of IPR even for the cases where quasiparticles are present. This fact confirms the trend that suggests that C-GNRs are good conductors[48] owing to fact that the more delocalized the charge carriers, the greater their mobilities. The figure is clear in indicating the critical value of 5.0 eV/Å in determining two distinct physical pictures for the charge transport trend: a delocalized picture and a quasiparticle-mediated regime. Below this value, one has a completely delocalized scenario (Figure 3b). Above it, charge localization

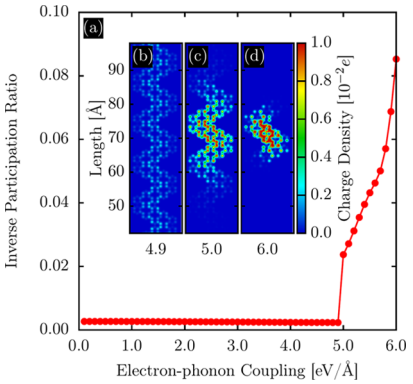

Figure 3. (a) Inverse participation ratio as a function of the electron−phonon coupling constant. (b−d) Charge distribution for small, critical, and large α, respectively.

takes place in the form of quasiparticles, as can be inferred from Figure 3c,d.

Figure 3b−d presents the profile of charge concentration for three different electron−phonon coupling constants, i.e., 4.9 eV/Å (complete delocalization), 5.0 eV/Å (critical value), and 6.0 eV/Å (localized charge). Simulations with α smaller than 4.9 eV/Å yield the same profile, as can be seen in (a), i.e., a null IPR is achieved in all cases. From 5.0 eV/Å on, the localization degree monotonically increases and a quasiparticle scenario is always observed. The high value of 6.0 eV/Å is associated with a correspondingly high IPR. This should have a large impact on the charge mobility of the particular system. However, one should be most interested in values slightly higher than 5.0 eV/Å, as this constant corresponds to the experimentally observed band gap value.

A natural question that arises is whether the same behavior is observed when a more charged system is considered. To investigate this trend, we consider an electron−phonon coupling regime smaller than the critical value. Figure 4 corresponds to C-GNRs in which α = 4.5 eV/Å is considered.

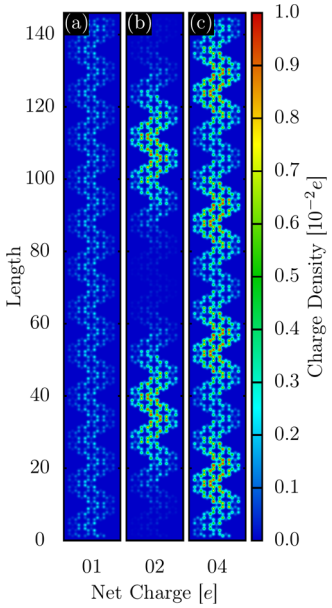

Figure 4. Atomic charge distribution for α = 4.5 eV/Å in the case of one, two, and four holes in the system.

https://dx.doi.org/10.1021/acs.jpcc.0c06625
J. Phys. Chem. C 2020, 124, 22392−22398

In Figure 4a, we have one positive charge carrier in the system. As this value is below the 5.0 eV/Å threshold, the result is a completely delocalized picture, indistinguishable from that in Figure 3b. The situation is drastically altered when two charge carriers are considered, as in Figure 4b. Note that, in this case, even though α < 5.0 eV/Å, a clear charge localization in two centers is observed. In Figure 4c, we include four holes in the system and, again, one can see the charge distribution typical of quasiparticles. In this case, because of the size of the nanoribbons, the four quasiparticles cover the whole extension of its length. The periodic disposition of variable amounts of charge, however, leaves no room for doubt: far from being a delocalized evenly displaced scenario as in Figure 4a, we have four equally spaced charge carriers. From this set of simulations, we conclude that the critical value that separates delocalized and localized scenarios is highly dependent on the amount of charge. Highly charged C-GNRs tend to favor a charge carrier mediated transport over a delocalized picture.

We now focus our attention on the experimentally expected value of α = 5.2 eV/Å. The idea here is to study the system with different quasiparticle scenarios. Figure 5a presents the

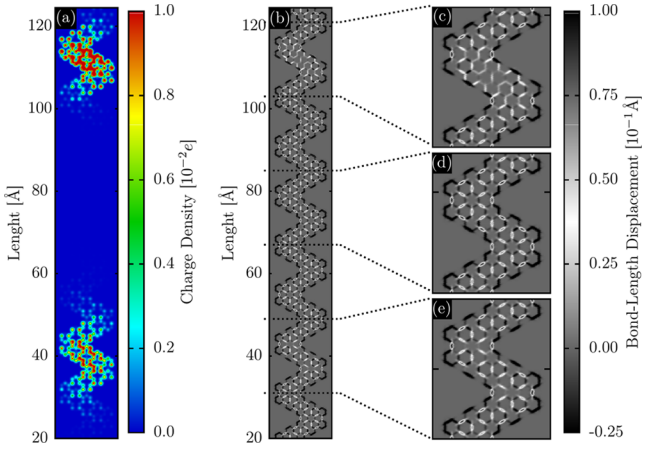

Figure 5. Ground sate (stationary) solution for a C-GNR lattice containing a polaron and a bipolaron. Panels (a) and (b) illustrate the charge density and bond length profiles. Panels (c−e) show zoom-in images of three distinct regions for the bond length configuration panel: (c) the region containing a bipolaron, (d) a region without additional charge, and (e) the region containing a polaron.

charge density localization of C-GNR with a polaron (charge localization signature between 20 and 60 Å) and a bipolaron (charge localization signature between 100 and 120 Å). Figure 5b−e, in turn, illustrates the respective bond length configuration. For the sake of clarity, Figure 5c−e shows zoom-in images of three distinct regions for the bond length configuration panel: (c) the region containing a bipolaron, (d) a region without additional charge, and (d) the region containing a polaron. By keeping a +2*e* net charge but considering the opposite spin we achieve the hole bipolaron in Figure 5a. Note the stronger red pattern when compared to the charge density for a bipolaron with a polaron, which is associated with twice the charge of the individual carrier of the latter. Importantly, in Figure 4b−e, one can realize that the charge localization signatures for a polaron and a bipolaron have related local lattice distortions. This behavior is a piece of evidence that two different structures are formed by a self-interacting state between extra charge and local lattice deformations. Moreover, one can note that the lattice distortions associated with the bipolaron present a different pattern in the case of polaron. This feature is attributed to the higher degree of charge localization as presented for the bipolaron case.

The dynamics of the charge carriers is presented in Figure 6. This analysis is crucial for defining the mobility and dynamical

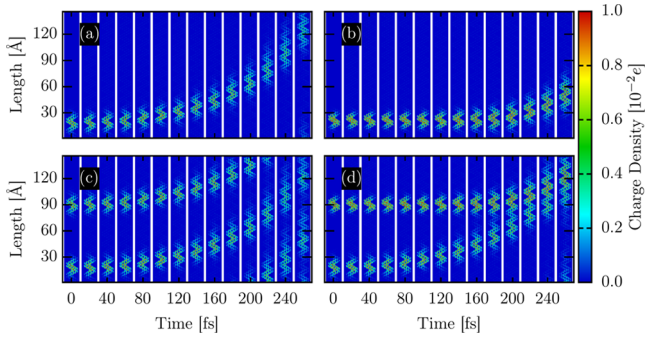

Figure 6. Dynamics of (a) polaron, (b) bipolaron, (c) pair of polarons, and (d) polaron and bipolaron on chevron-graphene nanoribbons under the influence of a 1.0 mV/Å electric field applied in the length direction.

stability of the carriers, which, in turn, impact the transport properties of the system. We investigate how each system behaves under the influence of a 1.0 mV/Å electric field. Figure 6a presents polaron dynamics. Note that after a transient period, the polaron begins to move as a result of the electric field. It should be remembered that the electric field is turned on adiabatically according to the approach in ref 40, thus the delay in the polaron response. In Figure 6b, we observe the dynamics of the bipolaron. More importantly, its response is accordingly slower and, although being more charged, results in a shorter displacement. Figure 6c presents two polaron simulations. As the quasiparticles are identical, their paths are parallel. Each one is similar to that given in Figure 6a. In this case, note that the periodic boundary conditions applied to the system: as the upper polaron reaches the top of the figure, it comes right back from its bottom. This does not happen for the polaron in the final Figure 6d. In this case, we present the simulation in which both polaron and bipolaron are present. The aforementioned difference of inertia and the consequent difference in response to the applied field becomes clear, as the bipolaron barely moves 30 Å, while, at the same time, the same electric field causes the polaron to displace more than 80 Å. Also, note that a collision takes place between the faster polaron and the slower bipolaron, which prevents the former from achieving the edge of the nanoribbon, as shown in Figure 6c.

As mentioned above, polarons and bipolarons move in the lattice as a composited state formed by the self-interaction between the additional charge and related local lattice distortions. To show this feature, Figure 7 presents the bipolaron dynamics corresponding to Figure 6b. The yellow rectangles serve as a guide for the eye in following the bipolaron's bond length displacements. In this way, in Figure 7, one can note that the local lattice distortions move by following the charge density motion. This dynamic trend is similar to those of the other cases discussed here (Figure 6a,c,d). Therefore, the combined analyses of Figures 6 and 7 show that in C-GNRs the composite quasiparticles are

https://dx.doi.org/10.1021/acs.jpcc.0c06625
J. Phys. Chem. C 2020, 124, 22392−22398

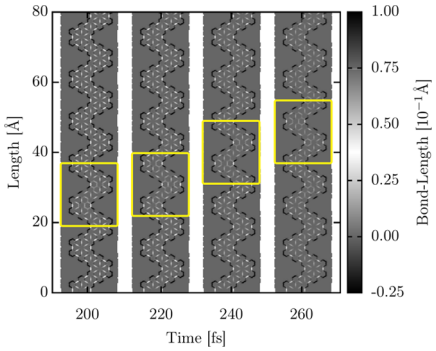

Figure 7. Time evolution for the bond length configuration of the bipolaron dynamics presented in Figure 6b. The yellow rectangles serve as a guide for the eye to follow the bipolaron's bond length displacements.

dynamically stable once charge and related lattice deformations move together as a single structure.

As can be inferred from Figure 6, after a transient period for acceleration, both charge carriers reach their saturation velocities. These terminal velocities are in the interval range of 0.05−0.75 and 0.001−0.36 Å/fs for the polaron and bipolaron cases, respectively. When it comes to standard armchair graphene nanoribbons, the terminal velocities of polarons and bipolarons are within the interval range of 0.3−5.1[49] and 0.05−1.30 Å/fs,[43] respectively, depending on the ribbon's width and the strength of the applied electric field. Importantly, the similarities in terminal velocities among C-GNRs and standard armchair graphene nanoribbons come from their comparable charge localization profiles that yield quasiparticles with equivalent effective masses. Figure 9 illustrates the interplay between the terminal velocities of the charge carriers and the applied electric field strength. One can observe a linear relationship between these two quantities. The curve fitting shows that the polaron (μ_p) and bipolaron (μ_{bp}) mobilities in our model lattices are 46.51 ± 6.5 and 23.87 ± 7.7 $cm^2/(V\ s)$, respectively.

Finally, we present in Figure 8 the time evolution profile of the intragap energy levels of the simulations shown in Figure 6. For the sake of convenience, this figure illustrates only the first 100 fs of the carriers' dynamics. The blue and red intragap levels refer to the polaron and bipolaron species, respectively. In Figure 8a−d one can note that the quasiparticle levels remain within the band gap during the dynamics. This behavior is one more piece of evidence suggesting that polarons and bipolarons are dynamically stable in C-GNRs. The bipolaron levels are positioned narrower within the band gap, indicating that bipolarons are more stable species than polarons. Such a trend in the quasiparticles stability was also found for standard armchair graphene nanoribbons (Figure 9).[43]

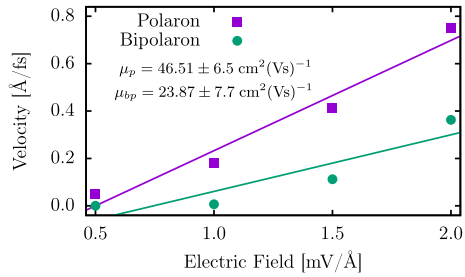

Figure 9. Charge carrier velocities as a function of the applied electric field for the C-GNR.

CONCLUSIONS

We have carried out an extensive investigation of the static and dynamic properties of different quasiparticles in chevron-graphene nanoribbons. Our computational protocol is based on a 2D tight-binding Hamiltonian that includes lattice relaxation effects. The reported results were observed to be rather different from those described for standard graphene nanoribbons, which may pave the way for different applications. The influence of the electron−phonon coupling on the conduction mechanism was explored. Here, we have obtained 5.2 eV/Å as the electron−phonon coupling strength corresponding to the expected 2.28 eV band gap for C-GNRs. This value is close to the critical value that determines two distinct physical pictures for the charge transport mechanism: a delocalized charge and a quasiparticle transport. We characterized and performed a detailed analysis of the dynamics of different charge carriers (polarons and bipolarons). By means of these results, we were able to determine the kind of quasiparticle presenting higher mobility. The terminal velocities for polarons and bipolarons in C-GNR lattices are 0.4 and 0.12 Å/fs, respectively. These velocities are similar to what is found for standard armchair graphene nanoribbons. The time evolution for the intragap energy levels suggests that

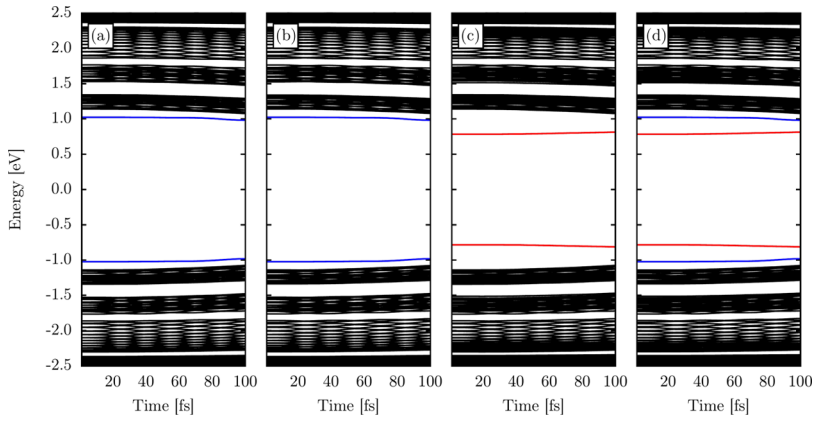

Figure 8. Time evolution profile of the intragap energy levels of simulations shown in Figure 6.

https://dx.doi.org/10.1021/acs.jpcc.0c06625
J. Phys. Chem. C 2020, 124, 22392−22398

polarons and bipolarons are dynamically stable in C-GNRs. Particularly, the bipolaron levels are positioned more narrowly within the band gap, indicating that this species is more stable than polarons.

■ ASSOCIATED CONTENT

Supporting Information

The Supporting Information is available free of charge at https://pubs.acs.org/doi/10.1021/acs.jpcc.0c06625.

Material presents the results obtained for the stability and transport of polarons and bipolarons in the E-GNR systems (PDF)

■ AUTHOR INFORMATION

Corresponding Author

Luiz Antônio Ribeiro Junior − *Institute of Physics, University of Brasília, 70919-970, Brazil*; orcid.org/0000-0001-7468-2946; Email: ribeirojr@unb.br

Authors

Marcelo Lopes Pereira Júnior − *Institute of Physics, University of Brasília, 70919-970, Brazil*

Wiliam Ferreira da Cunha − *Institute of Physics, University of Brasília, 70919-970, Brazil*; orcid.org/0000-0002-4163-9025

Rafael Timóteo de Sousa Junior − *Department of Electrical Engineering, University of Brasília, 70919-970, Brazil*

William Ferreira Giozza − *Department of Electrical Engineering, University of Brasília, 70919-970, Brazil*

Geraldo Magela e Silva − *Institute of Physics, University of Brasília, 70919-970, Brazil*

Complete contact information is available at: https://pubs.acs.org/10.1021/acs.jpcc.0c06625

Notes

The authors declare no competing financial interest.

■ ACKNOWLEDGMENTS

The authors gratefully acknowledge the financial support from the Brazilian Research Councils CNPq, CAPES, and FAP-DF and CENAPAD-SP for providing the computational facilities. M.L.P.J. gratefully acknowledges the financial support from the CAPES grant 88882.383674/2019-01. L.A.R.J. and W.F.G. gratefully acknowledge the financial support from the FAP-DF grant 0193.0000248/2019-32. L.A.R.J. and G.M.S gratefully acknowledge, respectively, the financial support from the CNPq grants 302236/2018-0 and 304637/2018-1, respectively. R.T.S.J. gratefully acknowledges the financial support from the CNPq grants 465741/2014-2 and 312180/2019-5, CAPES grant 88887.144009/2017-00, and FAP-DF grants 0193.001366/2016 and 0193.001365/2016.

■ REFERENCES

(1) Novoselov, K. S.; Geim, A. K.; Morozov, S. V.; Jiang, D.; Zhang, Y.; Dubonos, S. V.; Grigorieva, I. V.; Firsov, A. A. Electric Field Effect in Atomically Thin Carbon Films. *Science* **2004**, *306*, 666−669.

(2) Geim, A.; Novoselov, K. The rise of graphene. *Nat. Mater.* **2007**, *6*, 183−191.

(3) Polsen, E.; McNerny, D.; Balakrishnan, V.; Pattinson, S.; Hart, A. J. High-speed roll-to-roll manufacturing of graphene using a concentric tube CVD reactor. *Sci. Rep.* **2015**, *5*, No. 10257.

(4) Liu, M.; Yin, X.; Ulin-Avila, E.; Geng, B.; Zentgraf, T.; Ju, L.; Wang, F.; Zhang, X. A graphene-based broadband optical modulator. *Nature* **2011**, *474*, 64−67.

(5) Novoselov, K. Mind the gap. *Nat. Mater.* **2007**, *6*, 720−721.

(6) Zhou, S. Y.; Gweon, G.-H.; Fedorov, A. V.; First, P. N.; Heer, W. A.; Lee, D.-H.; Guinea, F.; Castro Neto, A. H.; Lanzara, A. Substrate-induced Bandgap Opening in Epitaxial Graphene. *Nat. Mater.* **2007**, *6*, 770−775.

(7) Szirmai, P.; Márkus, B. G.; Dóra, B.; Fábián, G.; Koltai, J.; Zólyomi, V.; Kurti, J.; Náfrádi, B.; Forró, L.; Pichler, T.; et al. Doped carbon nanotubes as a model system of biased graphene. *Phys. Rev. B* **2017**, *96*, No. 075133.

(8) Jiao, L.; Zhang, L.; Wang, X.; Diankov, G.; Dai, H. Narrow graphene nanoribbons from carbon nanotubes. *Nature* **2009**, *458*, 877−880.

(9) Xie, X.; Ju, L.; Feng, X.; Sun, Y.; Zhou, R.; Liu, K.; Fan, S.; Li, Q.; Jiang, K. Controlled Fabrication of High-Quality Carbon Nanoscrolls from Monolayer Graphene. *Nano Lett.* **2009**, *9*, 2565−2570.

(10) Wang, S.; Yang, B.; Chen, H.; Ruckenstein, E. Popgraphene: a new 2D planar carbon allotrope composed of 5-8-5 carbon rings for high-performance lithium-ion battery anodes from bottom-up programming. *J. Mater. Chem. A* **2018**, *6*, 6815−6821.

(11) Wang, Z.; Zhou, X.-F.; Zhang, X.; Zhu, Q.; Dong, H.; Zhao, M.; Oganov, A. R. Phagraphene: a low-energy graphene allotrope composed of 5-6-7 carbon rings with distorted dirac cones. *Nano Lett.* **2015**, *15*, 6182−6186.

(12) Zhang, S.; Zhou, J.; Wang, Q.; Chen, X.; Kawazoe, Y.; Jena, P. Penta-graphene: A new carbon allotrope. *Proc. Natl. Acad. Sci. U.S.A.* **2015**, *112*, 2372−2377.

(13) Teeter, J. D.; Zahl, P.; Mehdi Pour, M.; Costa, P. S.; Enders, A.; Sinitskii, A. On-Surface Synthesis and Spectroscopic Characterization of Laterally Extended Chevron Graphene Nanoribbons. *ChemPhysChem* **2019**, *20*, 2281−2285.

(14) Pour, M. M.; Lashkov, A.; Radocea, A.; Liu, X.; Sun, T.; Lipatov, A.; Korlacki, R. A.; Shekhirev, M.; Aluru, N. R.; Lyding, J. W.; et al. Laterally extended atomically precise graphene nanoribbons with improved electrical conductivity for efficient gas sensing. *Nat. Commun.* **2017**, *8*, No. 820.

(15) Costa, P. S.; Teeter, J. D.; Enders, A.; Sinitskii, A. Chevron-based graphene nanoribbon heterojunctions: Localized effects of lateral extension and structural defects on electronic properties. *Carbon* **2018**, *134*, 310−315.

(16) Radocea, A.; Sun, T.; Vo, T. H.; Sinitskii, A.; Aluru, N. R.; Lyding, J. W. Solution-synthesized chevron graphene nanoribbons exfoliated onto H: Si (100). *Nano Lett.* **2017**, *17*, 170−178.

(17) Lee, Y.-L.; Zhao, F.; Cao, T.; Ihm, J.; Louie, S. G. Topological Phases in Cove-Edged and Chevron Graphene Nanoribbons: Geometric Structures, Z 2 Invariants, and Junction States. *Nano Lett.* **2018**, *18*, 7247−7253.

(18) Teeter, J. D.; Costa, P. S.; Pour, M. M.; Miller, D. P.; Zurek, E.; Enders, A.; Sinitskii, A. Epitaxial growth of aligned atomically precise chevron graphene nanoribbons on Cu (111). *Chem. Commun.* **2017**, *53*, 8463−8466.

(19) Vo, T. H.; Shekhirev, M.; Kunkel, D. A.; Orange, F.; Guinel, M. J.-F.; Enders, A.; Sinitskii, A. Bottom-up solution synthesis of narrow nitrogen-doped graphene nanoribbons. *Chem. Commun.* **2014**, *50*, 4172−4174.

(20) Cai, J.; Ruffieux, P.; Jaafar, R.; Bieri, M.; Braun, T.; Blankenburg, S.; Muoth, M.; Seitsonen, A.; Saleh, M.; Feng, X.; et al. Atomically Precise Bottom-up Fabrication of Graphene Nanoribbons. *Nature* **2010**, *466*, 470−473.

(21) Vo, H.; Shekhirev, M.; Kunkel, D.; Morton, M.; Berglund, E.; Kong, L.; Wilson, P.; Dowben, P.; Enders, A.; Sinitskii, A. Large-scale solution synthesis of narrow graphene nanoribbons. *Nat. Commun.* **2014**, *5*, No. 3189.

(22) Deniz, O.; Sánchez-Sánchez, C.; Jaafar, R.; Kharche, N.; Liang, L.; Meunier, V.; Feng, X.; Müllen, K.; Fasel, R.; Ruffieux, P. Electronic

characterization of silicon intercalated chevron graphene nanoribbons on Au (111). *Chem. Commun.* **2018**, *54*, 1619−1622.
(23) Smith, S.; Llinás, J.-P.; Bokor, J.; Salahuddin, S. Negative differential resistance and steep switching in chevron graphene nanoribbon field-effect transistors. *IEEE Electron Device Lett.* **2018**, *39*, 143−146.
(24) Lv, Y.; Ye, S.; Wang, H.; He, J.; Huang, Q.; Chang, S. Strain engineering of chevron graphene nanoribbons. *J. Appl. Phys.* **2019**, *125*, No. 082501.
(25) Lv, Y.; Huang, Q.; Chang, S.; Wang, H.; He, J.; Liu, A.; Ye, S.; Wang, W. Activating impurity effect in edge nitrogen-doped chevron graphene nanoribbons. *J. Phys. Commun.* **2018**, *2*, No. 045028.
(26) Wang, S.; Wang, J. Quasiparticle energies and optical excitations in chevron-type graphene nanoribbon. *J. Phys. Chem. C* **2012**, *116*, 10193−10197.
(27) Dollfus, P.; Nguyen, V. H.; Saint-Martin, J. Thermoelectric effects in graphene nanostructures. *J. Phys.: Condens. Matter* **2015**, *27*, No. 133204.
(28) Vo, T. H.; Shekhirev, M.; Lipatov, A.; Korlacki, R. A.; Sinitskii, A. Bulk properties of solution-synthesized chevron-like graphene nanoribbons. *Faraday Discuss.* **2014**, *173*, 105−113.
(29) Cai, J.; Pignedoli, C.; Talirz, L.; Ruffieux, P.; Söde, H.; Liang, L.; Meunier, V.; Berger, R.; Li, R.; Feng, X.; et al. Graphene nanoribbon heterojunctions. *Nat. Nanotechnol.* **2014**, *9*, 896−900.
(30) Su, W. P.; Schrieffer, J. R.; Heeger, A. J. Soliton excitations in polyacetylene. *Phys. Rev. B* **1980**, *22*, 2099−2111.
(31) Su, W. P.; Schrieffer, J. R.; Heeger, A. J. Solitons in Polyacetylene. *Phys. Rev. Lett.* **1979**, *42*, 1698−1701.
(32) da Cunha, W. F.; Acioli, P. H.; de Oliveira Neto, P. H.; Gargano, R.; e Silva, G. M. Polaron properties in armchair graphene nanoribbons. *J. Phys. Chem. A* **2016**, *120*, 4893−4900.
(33) Barone, V.; Hod, O.; Scuseria, G. E. Electronic structure and stability of semiconducting graphene nanoribbons. *Nano Lett.* **2006**, *6*, 2748−2754.
(34) de Oliveira Neto, P. H.; Teixeira, J.; da Cunha, W.; Gargano, R.; e Silva, G. Electron-lattice coupling in armchair graphene nanoribbons. *J. Phys. Chem. Lett.* **2012**, *3*, 3039−3042.
(35) Ribeiro, L. A., Jr.; da Cunha, W. F.; Fonseca, A. L. d. A.; e Silva, G. M.; Stafstrom, S. Transport of polarons in graphene nanoribbons. *J. Phys. Chem. Lett.* **2015**, *6*, 510−514.
(36) Kotov, V. N.; Uchoa, B.; Pereira, V. M.; Guinea, F.; Neto, A. C. Electron-electron interactions in graphene: Current status and perspectives. *Rev. Mod. Phys.* **2012**, *84*, No. 1067.
(37) Yan, J.; Zhang, Y.; Kim, P.; Pinczuk, A. Electric field effect tuning of electron-phonon coupling in graphene. *Phys. Rev. Lett.* **2007**, *98*, No. 166802.
(38) Neto, A. C.; Guinea, F.; Peres, N. M. R.; Novoselov, K. S.; Geim, A. K. Peres NMR, Novoselov KS, Geim AK The electronic properties of graphene. *Rev. Mod. Phys.* **2009**, *81*, No. 109.
(39) Yan, J.; Zhang, Y.; Goler, S.; Kim, P.; Pinczuk, A. Raman scattering and tunable electron-phonon coupling in single layer graphene. *Solid State Commun.* **2007**, *143*, 39−43.
(40) da Cunha, W. F.; de Oliveira Neto, P. H.; Terai, A.; e Silva, G. M. Dynamics of charge carriers on hexagonal nanoribbons with vacancy defects. *Phys. Rev. B* **2016**, *94*, No. 014301.
(41) da Cunha, W. F.; Junior, L. A. R.; de Aklmeida Fonseca, A. L.; Gargano, R.; e Silva, G. M. Impurity effects on polaron dynamics in graphene nanoribbons. *Carbon* **2015**, *91*, 171−177.
(42) Fischer, M. M.; Junior, L. A. R.; da Cunha, W. F.; de Sousa, L. E.; e Silva, G. M.; de Oliveira Neto, P. H. Ultrafast direct generation of quasiparticles in graphene nanoribbons. *Carbon* **2020**, *158*, 553−558.
(43) Silva, G. G.; Ribeiro, L. A.; Pereira Junior, M. L.; de Almeida Fonseca, A. L.; de Sousa Júnior, R. T.; Magela e Silva, G. Bipolaron Dynamics in Graphene Nanoribbons. *Sci. Rep.* **2019**, *9*, No. 2909.
(44) Júnior, M. L. P.; Neto, B. G. E.; Giozza, W. F.; de Sousa Junior, R. T.; e Silva, G. M.; Junior, L. A. R. Transport of Quasiparticles in Coronene-Based Graphene Nanoribbons. *J. Mater. Chem. C* **2020**, 12100−12107.
(45) da Cunha, W. F.; de Oliveira Neto, P. H.; Terai, A.; e Silva, A. G. M. Dynamics of charge carriers on hexagonal nanoribbons with vacancy defects. *Phys. Rev. B* **2016**, *94*, No. 014301.
(46) da Cunha, W. F.; de Oliveira Neto, P. H.; Junior, L. A. R.; e Silva, G. M. Quasiparticle description of transition metal dichalcogenide nanoribbons. *Phys. Rev. B* **2019**, *99*, No. 035405.
(47) Pereira, M. L.; da Cunha, W. F.; de Sousa, R. T.; e Silva, G. M.; Ribeiro, L. A. Stationary and Dynamical Properties of Polarons in Anisotropic C60-Crystals. *J. Phys. Chem. C* **2019**, *123*, 13410−13418.
(48) Vo, T. H.; Shekhirev, M.; Lipatov, A.; Korlacki, R.; Sinitskii, A. Bulk properties of solution-synthesized chevron-like graphene nanoribbons. *Faraday Discuss.* **2014**, *173*, 105−113.
(49) Silva, G. G.; da Cunha, W. F.; de Sousa Junior, R. T.; Almeida Fonseca, A. L.; Ribeiro Júnior, L. A.; e Silva, G. M. Influence of quasiparticle density over polaron mobility in armchair graphene nanoribbons. *Phys. Chem. Chem. Phys.* **2018**, *20*, 16712−16718.

https://dx.doi.org/10.1021/acs.jpcc.0c06625
J. Phys. Chem. C 2020, 124, 22392−22398